

Journal of
Mechanics of
Materials and Structures

**TIME-DOMAIN THIN LAYER METHOD FOR COMPUTING
TRANSIENT RESPONSE DUE TO SUDDEN/MOVING LOADS**

Hirokazu Takemiya

Volume 3, N° 10

December 2008



mathematical sciences publishers

TIME-DOMAIN THIN LAYER METHOD FOR COMPUTING TRANSIENT RESPONSE DUE TO SUDDEN/MOVING LOADS

HIROKAZU TAKEMIYA

In this study, the author applied the thin-layer method (TLM) for developing explicit time domain solutions for the ground response due to impulse and moving loads. The Fourier and Laplace transforms for space and time, respectively, are applied to derive the transformed domain solution that satisfies given boundary conditions. The eigenvalue decomposition in the Laplace parameter domain and the discrete wave number superposition for the horizontal wave field description lead to an accurate and efficient strategy for a stable time-space domain solution. Some demonstrations are given: The first example is a fundamental problem relating to interpretation of the causal transient responses of the P, S, and Rayleigh waves due to an impact loading. The second example is also fundamental, and treats the description of a compound wave field produced by a single moving load, detailing the kinematic as well as the inertial effects, with the speed being an important parameter. The third example is an engineering application that demonstrates the track response due to train passage in order to interpret the wave generation in ground by the high-speed passage. A comparison to measurement data is presented for validation.

1. Introduction

In the 1950s, the importance of studies on the transient and stationary responses of an elastic medium under impact/moving loads was recognized, and analytical solutions to these problems were derived under special conditions. These solutions have provided information to learn about the relevant wave field. Further, they can lead to fundamental solutions to solve the more complicated engineering problem by the modern numerical methods.

Regarding fixed position loading on an elastic halfspace medium, there exists a classical work by Lamb [1904] for a time harmonic problem which includes an attempt for a transient response by using the Fourier series expansion. An impulse problem of a vertical point load was solved by Pekeris [1955] for the surface response by applying the Laplace transform and the inverse of the transform solution in the complex plane. Mitra [1964] applied the same method for a disc-type impulse load. Eason [1966] applied the inverse Laplace transform by a suitable complex number contour integration, leaving some infinite integrals that contain the Bessel function for all points of the solid. In the wave fields, the causality of respective wave propagation is of primary interest. By using those obtained Green functions, the initial-boundary value problems have been solved in the time domain boundary method step-by-step [Takemiya and Steinfeld 1993; Takemiya and Fujiwara 1994; Takemiya et al. 1994].

Regarding moving loads on an elastic halfspace medium, classical work has been done by applying the integral transform method. Eason [1965] considered a three-dimensional problem for a moving force

Keywords: transient response, causality, impulse load, moving load, thin layer method, Laplace–Fourier transform, time domain solution, high-speed train.

This work was done while the author worked at Okayama University, Okayama, Japan.

with a constant speed on a homogeneous semi-infinite space (halfspace), deriving the stationary solution in the range less than the Rayleigh wave speed. Using the Betti–Rayleigh reciprocal theorem, Payton [1964] dealt with a transient problem of the sudden application of a load and subsequent movement at constant velocity on an elastic halfspace. Gakenheimer and Miklowitz [1969] employed the Laplace transform for time and then applied the Cagniard method for the inversion of the transformed solution. They discussed the transient response for three different states in terms of the speed ratio of the moving load velocity against the seismic P and S wave velocities. A constant moving velocity constitutes a stationary problem with the relative coordinates of $x - ct$ where x is distance, t is time and c is the velocity of the moving load. Recently, such a moving load problem has been advanced in the study of ground motions induced by a high-speed train [Dieterman and Metrikine 1997; Sheng et al. 1999; Lombaert et al. 2001; Takemiya 2003; Takemiya and Bian 2005].

As an idealization of the ground, a halfspace has been employed for the sake of closed form solution that allows for the interpretation of surface wave propagation. However, in view of actual situations in which soft surface soil is deposited on hard soil, a layer or a layered halfspace may be a more useful model for interpreting the observed dispersive wave field. In the studies of seismic wave synthesis, a vertically heterogeneous model has been proposed. The finite element discretization is taken in the direction of depth by Lysmer and Drake [1972] for the Rayleigh wave analysis.

For the three-dimensional problem, Olson et al. [1984] attempted to apply the wave number decomposition for the horizontal dependence of the wave motion to the layered system. This formulation, specially termed a *thin layer method* (TLM) by Kausel et al. [1975], is used to evaluate the extending soil effects in the soil-foundation dynamic analysis. The frequency domain formulation results in a set of algebraic governing equations of wave numbers. If a rigid base underlies the layers, general eigenvalue determination programs are straightforwardly available for the solution. The eigenvalue decomposition enables the wave number integral operation in a closed form by residue theory. This corresponds to solving the locked modes in the layered halfspace, as stated in Harvey [1981], discarding the leaking modes that Haddon [1987] discussed.

For the former situation, an alternative approach is shown by Kausel [1994] and Touhei [1995] by taking the closed form inverse Fourier transform for time with a set of discrete wave number superimpositions for space. To fulfill the required causality of wave propagation, Takemiya and Goda [2000] applied the Laplace transform instead in the seismic fault rupture problem.

In this paper, by applying the Fourier and Laplace transforms to time and space, respectively, to the layered ground model, the direct time domain solution is obtained with special attention paid to the initial condition for the wave propagation. The Laplace transform scheme surpasses the Fourier transform regarding the causality arguments [Takemiya and Guan 1993].

Firstly, the response of a halfspace medium under a sudden loading on the surface is investigated with respect to the wave front propagation in time. The accuracy of the thin layer solution is checked by comparison to the closed form solution. Secondly, the moving load problem on an elastic stratum with the initial condition and the stationary without it are compared. We focus on the effect of the moving speed on the predominant wave velocity of the medium as a crucial parameter. The causal wave generation, given a starting position, is discussed in reference to the frequency domain solution. Thirdly, for validating the present procedure, wave synthesis is attempted for train loading to compare to the measurement data under the low- and high-speed passages.

2. Solution method by Fourier–Laplace transform

The equation of motion governing elastodynamics is given by

$$\mu u_{i,jj} + (\lambda + \mu)u_{j,ji} + \rho \ddot{u}_i = f_i, \tag{1}$$

where λ and μ define the Lamé constants, ρ is the density, u is the displacement, f is the body force action, and \ddot{u} denotes the double differentiation of u with respect to time t . The subscripts i and j correspond to the Cartesian coordinates x , y , and z . Equation (1) can be reformulated in the Fourier transform technique as

$$\tilde{\tilde{u}}(\xi_x, \xi_y, z, s) = \int_{-\infty}^{\infty} \int_{-\infty}^{\infty} \int_0^{\infty} u(x, y, z, t) \exp(-st) \exp(i\xi_x x) \exp(i\xi_y y) dt dx dy, \tag{2}$$

$$u(x, y, z, t) = \frac{1}{8\pi^3 i} \int_{-\infty}^{\infty} \int_{-\infty}^{\infty} \int_{\sigma-i\infty}^{\sigma+i\infty} \tilde{\tilde{u}}(\xi_x, \xi_y, z, s) \exp(pt) \exp(-i\xi_x x) \exp(-i\xi_y y) ds d\xi_x d\xi_y, \tag{3}$$

where the symbols $\tilde{\tilde{}}$ and $\tilde{\tilde{}}$ define the Fourier transform with respect to space coordinates and the Laplace transform with respect to time, respectively; the notations ξ_x and ξ_y are the wave numbers along the x and y directions respectively; and i is an imaginary unit.

The associated equation is then coordinate transformed by

$$\begin{Bmatrix} \tilde{\tilde{u}}_x \\ \tilde{\tilde{u}}_y \\ \tilde{\tilde{u}}_z \end{Bmatrix} = \begin{bmatrix} i\xi_x/\xi & 0 & -i\xi_y/\xi \\ i\xi_y/\xi & 0 & i\xi_x/\xi \\ 0 & 1 & 0 \end{bmatrix} \begin{Bmatrix} \tilde{\tilde{u}}_1 \\ \tilde{\tilde{u}}_2 \\ \tilde{\tilde{u}}_3 \end{Bmatrix}, \quad \text{or} \quad \tilde{\tilde{u}}_{x,y,z} = D\tilde{\tilde{u}}_{1,2,3}, \tag{4}$$

where $\xi = \sqrt{(\xi_x^2 + \xi_y^2)}$. The subscripts 1, 2, and 3 correspond to the new orientations after the coordinate transformation. The associated vector transformation holds for the forces also.

$$\tilde{\tilde{f}}_{x,y,z} = D\tilde{\tilde{f}}_{1,2,3}. \tag{5}$$

The coordinate transformation of (4) polarizes the three-dimensional governing (1) into an expression for the in-place wave field comprising the P and SV waves and one for the out-of-plane wave field comprising the SH wave. Then, the respective governing equations are

$$\begin{bmatrix} \mu & 0 \\ 0 & \lambda + 2\mu \end{bmatrix} \begin{Bmatrix} \frac{d^2 \tilde{\tilde{u}}_{1n}}{dz^2} \\ \frac{d^2 \tilde{\tilde{u}}_{2n}}{dz^2} \end{Bmatrix} + \begin{bmatrix} 0 & -(\lambda + \mu)\xi \\ (\lambda + \mu)\xi & 0 \end{bmatrix} \begin{Bmatrix} \frac{d\tilde{\tilde{u}}_{1n}}{dz} \\ \frac{d\tilde{\tilde{u}}_{2n}}{dz} \end{Bmatrix} + \begin{bmatrix} (\lambda + 2\mu)k_\alpha^2 & 0 \\ 0 & -\mu k_\beta^2 \end{bmatrix} \begin{Bmatrix} \tilde{\tilde{u}}_{1n} \\ \tilde{\tilde{u}}_{2n} \end{Bmatrix} + \begin{Bmatrix} \tilde{\tilde{f}}_{1n} \\ \tilde{\tilde{f}}_{2n} \end{Bmatrix} = \begin{Bmatrix} 0 \\ 0 \end{Bmatrix}, \tag{6}$$

$$\mu \frac{d^2 \tilde{\tilde{u}}_{3n}}{dz^2} - \mu k_\beta^2 \cdot \tilde{\tilde{u}}_{3n} + \tilde{\tilde{f}}_{3n} = 0, \tag{7}$$

where the notations $k_\alpha = \sqrt{\xi^2 + (p/V_p)^2}$ for the P wave number and $k_\beta = \sqrt{\xi^2 + (p/V_s)^2}$ for the S wave number are used.

The discretization of the displacement is employed by the thin layer elements. The use of a linear interpolation function Φ for the displacements of neighboring nodes leads to the matrix equations

$$(\mathbf{A}^{\text{P-SV}}\xi^2 + \mathbf{B}^{\text{P-SV}}\xi + \mathbf{C}^{\text{P-SV}} + s^2\mathbf{M}^{\text{P-SV}})\tilde{\mathbf{U}}_{123}^{\text{P-SV}} = \tilde{\mathbf{F}}_{123}^{\text{P-SV}}, \tag{8}$$

$$(\mathbf{A}^{\text{SH}}\xi^2 + \mathbf{C}^{\text{SH}} + s^2\mathbf{M}^{\text{SH}})\tilde{\mathbf{U}}_{123}^{\text{SH}} = \tilde{\mathbf{F}}_{123}^{\text{SH}}, \tag{9}$$

where $\tilde{\mathbf{U}}$ denotes the nodal displacements and $\tilde{\mathbf{F}}$ the nodal forces. The superscripts P-SV and SH indicate the wave field concerned; namely, the former refers to the in-plane motion of the P and SV waves and the latter to the out-of-plane motion of the SH wave. Note here that the above decoupled equations coincide with those formulated in cylindrical coordinates in such a way that the subscripts 1, 2, and 3 correspond to r , z , and θ , respectively. Therefore, the coefficient matrices \mathbf{A} , \mathbf{B} , \mathbf{C} , \mathbf{M} are described in detail in the original paper [Kausel et al. 1975]. Equations (8) and (9) can be taken as eigenvalue problems with respect to the Laplace parameter s , whose general expression is cast as

$$\{\hat{\mathbf{A}}^{\text{P-SV}} + s^2\mathbf{M}^{\text{P-SV}}\}\Phi_m^{\text{P-SV}} = 0, \tag{10}$$

$$\{\hat{\mathbf{A}}^{\text{SH}} + s^2\mathbf{M}^{\text{SH}}\}\Phi_m^{\text{SH}} = 0, \tag{11}$$

where $\hat{\mathbf{A}}^{\text{P-SV}} = \mathbf{A}^{\text{P-SV}}\xi^2 + \mathbf{B}^{\text{P-SV}}\xi + \mathbf{C}^{\text{P-SV}}$ and $\hat{\mathbf{A}}^{\text{SH}} = \mathbf{A}^{\text{SH}}\xi^2 + \mathbf{C}^{\text{SH}}$.

Equation (10) defines the generalized Rayleigh function for the in-plane wave and (11) the generalized Love waves for the out-of-plane wave by referring to the superscripts. The decomposed eigenvectors Φ satisfy the orthogonal condition:

$$\Phi_i^{\text{P-SV}}\mathbf{M}^{\text{P-SV}}\Phi_j^{\text{P-SV}} = \delta_{ij}, \tag{12}$$

$$\Phi_i^{\text{SH}}\mathbf{M}^{\text{SH}}\Phi_j^{\text{SH}} = \delta_{ij}, \tag{13}$$

$$(\Phi^{\text{P-SV}})^T\mathbf{A}^{\text{P-SV}}\Phi^{\text{P-SV}} = \mathbf{\Lambda}^{\text{P-SV}}, \tag{14}$$

$$(\Phi^{\text{SH}})^T\mathbf{A}^{\text{SH}}\Phi^{\text{SH}} = \mathbf{\Lambda}^{\text{SH}}, \tag{15}$$

$$\Phi^{\text{P-SV}} = [\phi_1^{\text{P-SV}}\phi_2^{\text{P-SV}}\dots\phi_{2n}^{\text{P-SV}}], \tag{16}$$

$$\Phi^{\text{SH}} = [\phi_1^{\text{SH}}\phi_2^{\text{SH}}\dots\phi_n^{\text{SH}}], \tag{17}$$

$$\mathbf{\Lambda}^{\text{P-SV}} = \text{diag}[-(s_i^{\text{P-SV}})^2], \quad (i = 1, 2, \dots, 2n), \tag{18}$$

$$\mathbf{\Lambda}^{\text{SH}} = \text{diag}[-(s_i^{\text{SH}})^2], \quad (i = 1, 2, \dots, n). \tag{19}$$

Therefore, using the eigenvectors above, the displacement and force vectors are represented as follows (where we've replaced superscript P-SV on Φ by subscript 1 and 2, and superscript SH by subscript 3):

$$\begin{Bmatrix} \tilde{\mathbf{U}}_1 \\ \tilde{\mathbf{U}}_2 \end{Bmatrix} = \begin{bmatrix} \Phi_1\bar{\mathbf{E}}^{\text{P-SV}}\Phi_1^T\Phi_1\bar{\mathbf{E}}^{\text{P-SV}}\Phi_1^T\Phi_1\bar{\mathbf{E}}^{\text{P-SV}}\Phi_2^T \\ \Phi_2\bar{\mathbf{E}}^{\text{P-SV}}\Phi_1^T\Phi_2\bar{\mathbf{E}}^{\text{P-SV}}\Phi_1^T\Phi_2\bar{\mathbf{E}}^{\text{P-SV}}\Phi_2^T \end{bmatrix} \begin{Bmatrix} \tilde{\mathbf{F}}_1 \\ \tilde{\mathbf{F}}_2 \end{Bmatrix}, \tag{20}$$

$$\mathbf{U}_3 = \left[\Phi_3\bar{\mathbf{E}}^{\text{SH}}\Phi_3^T\Phi_3\bar{\mathbf{E}}^{\text{SH}}\Phi_3^T \right] \begin{Bmatrix} \tilde{\mathbf{F}}_3 \end{Bmatrix}, \tag{21}$$

where

$$\bar{\mathbf{E}}^{\text{P-SV}} = \text{diag} \left\{ \frac{1}{(-s_j^{\text{P-SV}} + s^2)} \cdot \tilde{\mathbf{T}}(\xi_y, s) \right\}, \quad j = 1 \sim 2n, \tag{22}$$

$$\tilde{\mathbf{E}}^{\text{SH}} = \text{diag} \left\{ \frac{1}{(-s_j^{\text{SH}2} + s^2)} \cdot \bar{T}(\xi_y, s) \right\}, \quad j = 1 \sim n. \quad (23)$$

The term $\tilde{T}(\xi_y, s)$ defines the load effect, whose detailed description is given later. the wave number domain expressions for the load vectors are

$$\tilde{\mathbf{F}}_1 = \left[-i \frac{\xi_x}{\xi} \mathbf{I} - i \frac{\xi_y}{\xi} \mathbf{I} \right] \left\{ \begin{matrix} \tilde{\mathbf{F}}_x(\xi_x, \xi_y) \\ \tilde{\mathbf{F}}_y(\xi_x, \xi_y) \end{matrix} \right\}, \quad (24)$$

$$\tilde{\mathbf{F}}_2 = \tilde{\mathbf{F}}_z(\xi_x, \xi_y), \quad (25)$$

$$\tilde{\mathbf{F}}_3 = \left[-i \frac{\xi_y}{\xi} \mathbf{I} - i \frac{\xi_x}{\xi} \mathbf{I} \right] \left\{ \begin{matrix} \tilde{\mathbf{F}}_x(\xi_x, \xi_y) \\ \tilde{\mathbf{F}}_y(\xi_x, \xi_y) \end{matrix} \right\}, \quad (26)$$

where \mathbf{I} denotes a unit matrix. The expressions in (20) and (21) are now back transformed into the original Cartesian coordinates by using the transpose of the coefficient matrix of (4).

$$\begin{Bmatrix} \tilde{U}_x \\ \tilde{U}_y \\ \tilde{U}_z \end{Bmatrix} = \begin{bmatrix} \frac{\xi_x^2}{\xi^2} \Phi_1 \tilde{\mathbf{E}}^{\text{P-SV}} \Phi_1^T + \frac{\xi_y^2}{\xi^2} \Phi_3 \tilde{\mathbf{E}}^{\text{SH}} \Phi_3^T & \frac{\xi_x \xi_y}{\xi^2} \Phi_1 \tilde{\mathbf{E}}^{\text{P-SV}} \Phi_1^T - \frac{\xi_x \xi_y}{\xi^2} \Phi_3 \tilde{\mathbf{E}}^{\text{SH}} \Phi_3^T & i \frac{\xi_x}{\xi^2} \Phi_1 \tilde{\mathbf{E}}^{\text{P-SV}} \Phi_1^T \\ \frac{\xi_x \xi_y}{\xi^2} \Phi_1 \tilde{\mathbf{E}}^{\text{P-SV}} \Phi_1^T - \frac{\xi_x \xi_y}{\xi^2} \Phi_3 \tilde{\mathbf{E}}^{\text{SH}} \Phi_3^T & \frac{\xi_y^2}{\xi^2} \Phi_1 \tilde{\mathbf{E}}^{\text{P-SV}} \Phi_1^T + \frac{\xi_x^2}{\xi^2} \Phi_3 \tilde{\mathbf{E}}^{\text{SH}} \Phi_3^T & i \frac{\xi_y}{\xi^2} \Phi_1 \tilde{\mathbf{E}}^{\text{P-SV}} \Phi_1^T \\ -i \frac{\xi_x}{\xi^2} \Phi_2 \tilde{\mathbf{E}}^{\text{P-SV}} \Phi_1^T & -i \frac{\xi_y}{\xi^2} \Phi_2 \tilde{\mathbf{E}}^{\text{P-SV}} \Phi_1^T & \Phi_2 \tilde{\mathbf{E}}^{\text{P-SV}} \Phi_2^T \end{bmatrix} \times \begin{Bmatrix} \tilde{\mathbf{F}}_x(\xi_x, \xi_y) \\ \tilde{\mathbf{F}}_y(\xi_x, \xi_y) \\ \tilde{\mathbf{F}}_z(\xi_x, \xi_y) \end{Bmatrix}. \quad (27)$$

The horizontal loading generates the P-SV and SH waves while the vertical loading generates the P-SV but not the SH wave. The explicit expression for the analytical inverse Laplace transforms of the concerned elements $\tilde{\mathbf{E}}^{\text{P-SV}}$ and $\tilde{\mathbf{E}}^{\text{SH}}$ are given in the next section for given loading time functions $T(t)$.

The inverse Fourier transform of (3) can be replaced by the following stepwise numerical integration:

$$\mathbf{u}(x, y, z, N \Delta t) = \frac{1}{(2\pi)^2} \int_{-\infty}^{\infty} \int_{-\infty}^{\infty} \tilde{\mathbf{u}}(\xi_x, \xi_y, z, N \Delta t) e^{-i\xi_x x} e^{-i\xi_y y} d\xi_x d\xi_y, \quad (28)$$

where N is the number of the time increments Δt used for response duration. The odd and even nature of $\tilde{\mathbf{u}}(\xi_x, \xi_y, z, N \Delta t)$, when multiplied by $e^{-i\xi_x x} e^{-i\xi_y y}$, is used to our advantage to carry out the integral computation over $-\infty$ to $+\infty$ efficiently. The cylindrical coordinate transformation is employed further to make the integral operation more convenient since the wave number range over the distance ξ_r is truncated by certain discrete wave numbers, while that over the angle ξ_θ is limited to $0 \sim \pi/2$. Therefore,

$$\begin{aligned} \mathbf{u}(x, y, z, n \Delta t) &= \frac{1}{(2\pi)^2} \int_0^\infty \int_0^{2\pi} \tilde{\mathbf{u}}(\xi_r, \xi_\theta, z, n \Delta t) e^{-\xi_r \cos \xi_\theta} e^{\xi_r \sin \xi_\theta} \xi_r d\xi_r d\xi_\theta \\ &\cong \frac{1}{(2\pi)^2} \sum_{m=0}^{\pi/2} \sum_{n=0}^L \tilde{U}(\xi_{rn}, \xi_{\theta n}, z, N \Delta t) e^{-\xi_{rn} \cos \xi_{\theta n}} e^{\xi_{rn} \sin \xi_{\theta n}} \Delta \xi_r \Delta \xi_\theta, \end{aligned} \quad (29)$$

where L is the fundamental wavelength, $\Delta\xi_r = 2\pi/L$ and $\Delta\xi_\theta = \pi/2N$ are the wave number increments for the radius and angle, respectively, for which the total numbers N and M are used for superposition.

3. Modal transient responses due to certain surface loads

3.1. Space distribution. Consider a uniformly distributed surface load of unit intensity over $2b_x$ by $2b_y$ in the x - y plane which is either suddenly applied or impulsively applied at a fixed position. We can say that the the distribution along the x direction is given by $F_x(x)$, along the y direction by $F_y(x)$, and along the z direction by $\delta(z)$, and the intensity time variation is given by $T(t)$. Then,

$$F_i(x, y, z; t) = F_x(x)F_y(y)\delta(z) \cdot T(t). \tag{30}$$

The Fourier–Laplace transform of (30) is given by

$$\tilde{F}_i(\xi_x, \xi_y, s) = \tilde{F}_x(\xi_x)\tilde{F}_y(\xi_y) \cdot \bar{T}(s). \tag{31}$$

(a) *Uniform load.* A uniform load on the rectangular area is defined as

$$F_x(x) = [H(x + b_x) - H(x - b_x)] \iff \tilde{F}_x(\xi_x) = \frac{\sin(\xi_x b_x)}{\xi_x b_x}, \tag{32}$$

$$F_y(y) = [H(y + b_y) - H(y - b_y)] \iff \tilde{F}_y(\xi_y) = \frac{\sin(\xi_y b_y)}{\xi_y b_y}, \tag{33}$$

where the notation $H()$ defines a Heaviside function and the symbol \iff indicates Fourier transform pairs.

(b) *Load proportional to the deflection of an elastically supported beam.* Consider an elastically supported beam of the bending rigidity EI on Winkler springs whose stiffness is k per unit length along the y -axis but constant in width $2b_x$ in the x -direction. The base reaction of the Winkler springs is

$$F_z(x, y) = F_x(x) \cdot F_y(y) = \frac{1}{\sqrt{2}L_c} \exp\left(-\left|\frac{y}{L_c}\right|\right) \sin\left(\left|\frac{y}{L_c}\right| + \frac{\pi}{4}\right) \times \{H(x + b_x) - H(x - b_x)\}, \tag{34}$$

where $L_c = \sqrt[4]{4EI/k}$.

The Fourier transform of (34) is given by

$$F_z(\xi_x, \xi_y) = F_z(\xi_x) \cdot F_z(\xi_y) = \frac{4}{4 + (\xi_y L_c)^4} \cdot \frac{2 \sin \xi_x b_x}{\xi_x b_x}. \tag{35}$$

3.2. Time function.

(a) *Dirac type loading.* An impulse loading is defined by a Delta function $\delta()$. The Laplace transform pair is

$$T(t) = \delta(t) \iff \bar{T}(s) = 1. \tag{36}$$

(b) *Heaviside type loading.* A suddenly applied loading is expressed by a Heaviside function $H(t)$. The corresponding Laplace transform pair is

$$T(t) = H(t) \iff \bar{T}(s) = \frac{1}{s}. \tag{37}$$

(c) *Moving load.* A moving load with a space distribution $F_y(y)$ moving at constant speed c along the y -direction is considered. The mathematical expression is then

$$F_z(y - ct) \iff \tilde{F}(\xi_y)\tilde{T}(\xi_y, s), \tag{38}$$

where

$$\tilde{T}(\xi_y, s) = \frac{1}{s - i\xi_y c}. \tag{39}$$

The Laplace domain representation of the moving load has a similar nature as the modified Heaviside type loading but with a phase shift such that

$$\tilde{T}(\xi_y, t) = e^{i\xi_y ct}. \tag{40}$$

This expression indicates a specific periodicity in time by the train speed under a given site condition.

A loading consisting of N consecutive loads of intensities F_n ($n = 1, 2, \dots, N$) is expressed as

$$F_z(y - ct) = \sum_{n=0}^N F_n \delta(y - c \cdot n \Delta t), \tag{41}$$

so that the frequency domain counterpart becomes $\tilde{T}(\xi_y, n \Delta t) = e^{i\xi_y c \cdot n \Delta t}$. Further, in the case of a moving load accompanied by a harmonic oscillation of frequency ω_0 , the following expression holds:

$$F(y - ct) \exp(i\omega_0 t) \iff \tilde{F}_z(\xi_y)\tilde{\tilde{T}}(\xi_y, s), \tag{42}$$

where

$$\tilde{\tilde{T}}(\xi_y, s) = \frac{1}{s - i(\xi_y c - \omega_0)}. \tag{43}$$

The inverse Laplace transform is

$$\tilde{\tilde{T}}(\xi_y, t) = e^{i(\xi_y c - \omega_0)t}. \tag{44}$$

3.3. Eigenmode response. The transient responses of the decomposed modes are obtained from the inverse Laplace transforms of Equations (22) and (23) as

$$\mathbf{E}^{P-SV/SH} = \frac{1}{2\pi i} \int_{\gamma i - \infty}^{\gamma i + \infty} \text{diag} \left\{ \frac{1}{-(s_j^{P-SV/SH})^2 + s^2} \cdot \bar{T}(s) \right\} e^{st} ds, \tag{45}$$

which is evaluated from the residue theory for the respective loading types in the previous section. (Here $\mathbf{E}^{P-SV/SH}$ means that either subscript may be taken consistently across the equation.)

(a) *Dirac type loading.* Introducing Equation (45) for $\bar{T}(s)$ from Equation (36) results in the time domain solution. The damping effect is now taken into account by introducing the damping ratio β_j into each decomposed mode, taken as a system with a single degree of freedom. Then

$$\mathbf{E}^{P-SV/SH} = \text{diag} \left[\exp(-\beta_j s_j^{P-SV/SH} t) \frac{\sin(s_j^{P-SV/SH} t)}{s_j^{P-SV/SH}} \right]. \tag{46}$$

(b) *Heaviside type loading.* The response due to a suddenly applied (Heaviside type) loading is straightforwardly obtained by introducing $\bar{T}(s)$ from (36) into (45). However, we can alternatively evaluate it by integrating the Dirac's impulse response of (46). The result for the initial condition at rest is then:

$$E_H^{P-SV/SH}(t) = \text{diag} \left[\frac{1 - \exp(-\beta s_j^{P-SV/SH} t) \{ \beta \sin(s_j^{P-SV/SH} t) + \cos(s_j^{P-SV/SH} t) \}}{(\beta s_j^{P-SV})^2 + (s_j^{P-SV})^2} \right]. \tag{47}$$

(c) *Moving load.* For a moving oscillating load of a constant speed c in the y -direction with the frequency ω_0 , the inverse Laplace transform gives, after substituting (45) for $\bar{T}(\xi_y, s)$ from (43):

$$E^{P-SV/SH} = \text{diag} \frac{1}{(s_j^{P-SV/SH})^2 + (\beta s_j^{P-SV/SH} + i(\xi_y c - \omega_0))^2} \times \left(-\exp(-\beta s_j^{P-SV/SH} t) \beta \sin(s_j^{P-SV/SH} t) + \cos(s_j^{P-SV/SH} t) + \cos((\xi_y c - \omega_0)t) - i \left(\frac{\xi_y c - \omega_0}{s_j^{P-SV/SH}} \exp(-\beta s_j^{P-SV/SH} t) \sin(s_j^{P-SV/SH} t) - \sin((\xi_y c - \omega_0)t) \right) \right), \tag{48}$$

which has a dominant contribution along the line $\xi_y c = \omega_0$. Comparing (48) with (47) suggests that the latter response is reduced to the former response on this line. Therefore, at this resonant situation, the response due to a moving load turns out to be like that caused by a sudden Heaviside-type loading at the temporal position by the moving speed.

4. Laplace transform versus Fourier transform

We now discuss the correspondence between the Laplace transform and the Fourier transform. This will assist the interpretation of the results obtained using the first method described above. The formal conversion follows by substituting the Laplace parameter “ s ” with another parameter “ $i\omega$ ” of frequency ω multiplied by an imaginary unit i . Then, (30) becomes

$$F_i(x, y, z; \omega) = F_x(x) F_y(y) \delta(z) \cdot \bar{T}(\omega), \tag{49}$$

where the time function for the moving load (43) is expressed, after some manipulation, by

$$\bar{T}(\xi_y, \omega) = \frac{1}{c} \frac{i}{\left(\xi_y - \frac{\omega - \omega_0}{c} \right)} = \frac{2\pi}{c} \delta \left(\xi_y - \frac{\omega - \omega_0}{c} \right). \tag{50}$$

The $\delta()$ function involved indicates that the wave number along the moving direction of the load can be selected from the wave number-frequency domain solution as follows:

$$\xi_y = (\omega - \omega_0)/c. \tag{51}$$

The homogeneous equations (10) and (11) are replaced by

$$\{ \hat{A}^{P-SV} - \omega^2 M^{P-SV} \} \Phi_m^{P-SV} = 0, \tag{52}$$

$$\{ \hat{A}^{SH} - \omega^2 M^{SH} \} \Phi_m^{SH} = 0. \tag{53}$$

The solutions corresponding to in-plane and out-of-plane motions provide information on the wave number versus frequency characteristics of the respective eigenmodes. The inverse Fourier transforms with respect to wave numbers and frequency yield, in view of (51), the solution

$$u(x, y, z, t) = \frac{1}{(2\pi)^2 c} \int_{-\infty}^{\infty} \int_{-\infty}^{\infty} u\left(\xi_x, \frac{\omega - \omega_0}{c}, z, \omega\right) e^{-i\xi_x x} \cdot e^{i\left(\frac{\omega_0 y}{c}\right)} \cdot e^{i\omega\left(t - \frac{y}{c}\right)} d\xi_x d\omega. \quad (54)$$

Hence, the solution is characterized by the crossings of the wave number versus frequency diagrams of dispersive wave modes and the speed line of (51).

5. Computational results

5.1. Fundamental problem I: Transient response of a halfspace under a sudden loading. Investigated first is the transient response of an elastic isotropic homogeneous halfspace when a uniform disk load of a unit radius is impulsively applied (a Dirac-type loading) on the free surface. The schematic model is shown on the right. The properties are defined by the density ρ , the P wave and S wave velocities c_1 and c_2 , respectively, and the Poisson ratio ν . For the sake of the present TLM computation the halfspace is approximated by a stratum of the rigid base at 228 m deep, which is discretized by sub-layers as 10@0.4 m + 5@0.8 m + 10@1.0 m \times 10 + 10@2.0 m + 10@4.0 m \times 10 + 15@10 m. The fundamental wavelength is set to 700 m for the analysis. The discrete wave numbers for superposition are then set to 700. The time increment for response computation is $\Delta t = 10^{-3}$ [s]. The wave modes employed are 40 for in-plane motion and 20 for out-of-plane motion. These values yield a reliable solution with less computational time. The response observation points are as indicated in the figure to the right.

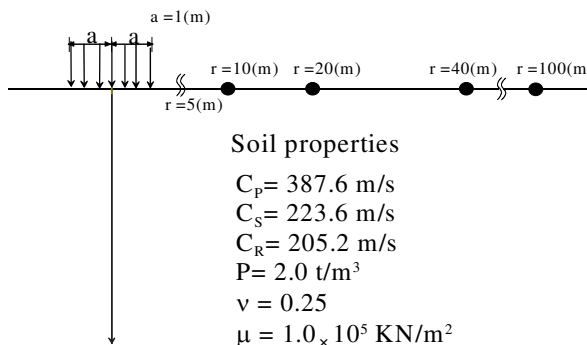


Figure 1. A halfspace under an impulse load.

The transient responses that reach the static displacements computed by the present method are depicted by symbols in Figure 2 in the dimensionless form. The response U_{ij} can be identified by the subscript ij with i indicating the response direction and j the loading direction. They are compared with analytical halfspace solutions by lines (denoted by HS) that are obtained by the author by following Eason’s formulation [1966] for the vertical loading. Since the Eason solution is limited to times after the S wave arrival, the author improved it as valid for all times. Further, the author extended it to the horizontal loading case to give an excellent match, when the loaded area is assumed small enough, with Pekeris’ solution [1955] for a point loading. The letters P , S and R are designated to indicate the wave front arrivals of the P , S and Rayleigh waves, respectively. A unit of dimensionless time corresponds to the arrival of the S wave at a focused point. The wave causality is noted to be clearly fulfilled in view of the respective wave front arrival times. An excellent agreement is attained between the present and the closed form solutions, as the focused point is at a far distance from the loading center. In Figure 2, the Rayleigh wave dominates the vertical and horizontal responses, whereas the P wave contribution appears small.

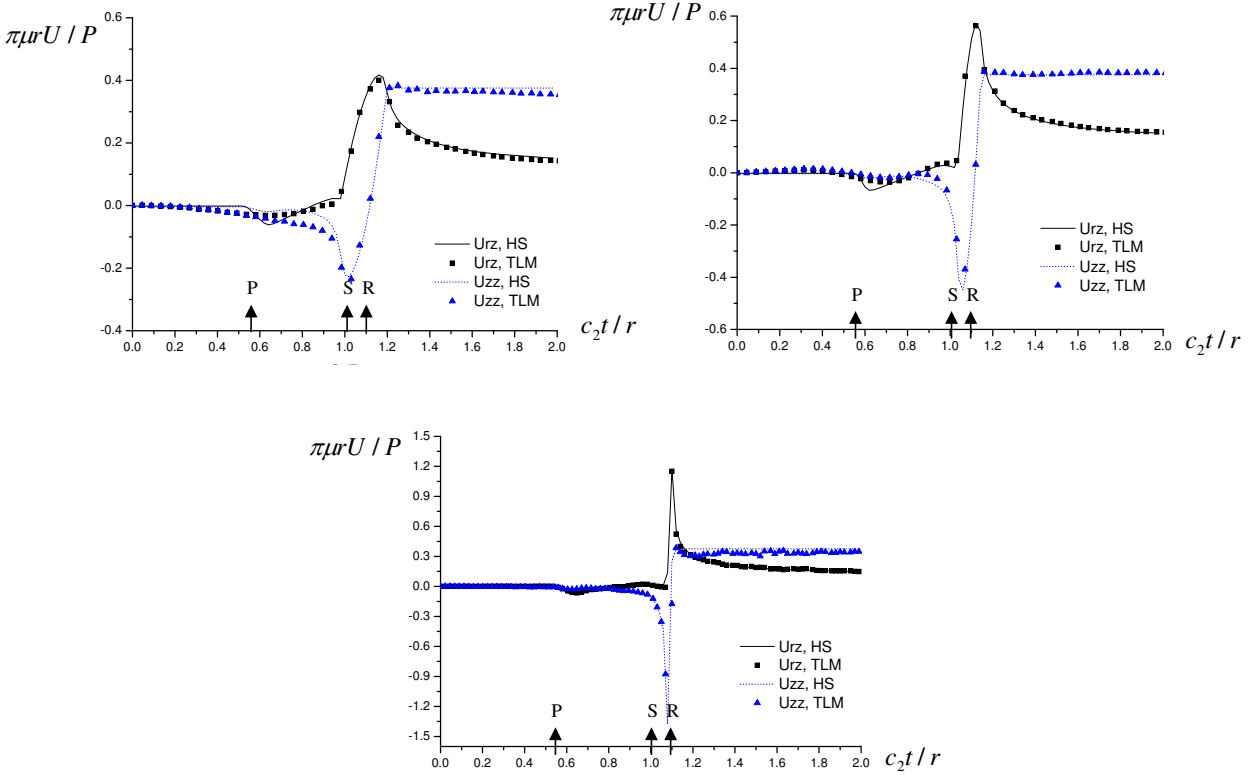


Figure 2. Transient response of a halfspace under a vertical disk load: horizontal (radial) and vertical at distances of 10 m (top left), 20 m (top right), and 100 m (bottom).

5.2. Fundamental problem II: Causality in a transient response for a moving load on a stratum. Comparison of the ground surface response is made between the moving Green functions from the Fourier Transform method [Takemiya 2001; Takemiya et al. 2001] that uses the wave propagation matrix across layers and the present direct Time Domain TLM. In order to investigate the wave field for a suddenly applied and then moving load, a simple stratum, as described in Figure 3, is employed for the model. The load and stratum properties are provided there. The sublayer division is made such that $20m=50@0.4$ m, which guarantees roughly the shortest wavelength of 2 m at the frequency 100 Hz since there exist 5 nodal points within it. A key consideration in the design of this investigation is the placement of the observation point at a location which allows the initial effect to be distinguished from the moving effect of the load.

First, the site characteristics are investigated by computing the wave dispersion curves in the form of the wave number versus frequency, and the group velocity versus frequency. They are depicted in Figure 4 (left and right, respectively). In layered soils, the wave generation is significantly affected by the so-called Airy phase frequency. These frequencies are noted at 4 Hz, 13 Hz, and 12 Hz, respectively, for the first, second, and third modes of the in-plane motions. The speed of the moving load is also important for the wave generation. Here, three representative situations, as defined by the speed ratio α of the moving load against the S wave velocity of the medium, are demonstrated: $\alpha < 1$ is the subseismic

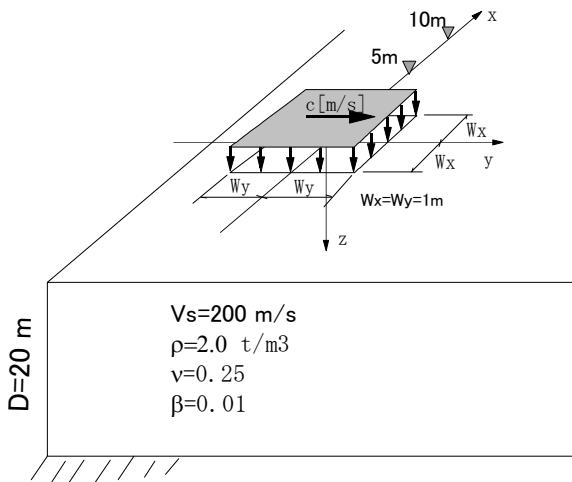


Figure 3. Stratrum model for analysis under a moving load.

condition, $\alpha = 1$ the seismic condition, and $\alpha > 1$ the superseismic condition. These are indicated in Figure 4 by the dashed lines as a parameter to locate which frequency is most associated with the wave generation. For the speed ratio $\alpha < 1$, there is no crossing with the dispersion curves; for $\alpha = 1$, the crossing of the speed line with the 1st mode occurs at 6 Hz; and for $\alpha = 2$, it occurs at 4 Hz.

The TLM computed responses at the ground surface are depicted in Figures 5–7. The distance between the starting position of the load and the observation point is taken as 40 m along the direction of motion, with and offset of either 5 m or 10 m perpendicular to the direction of motion. The numbers of wave

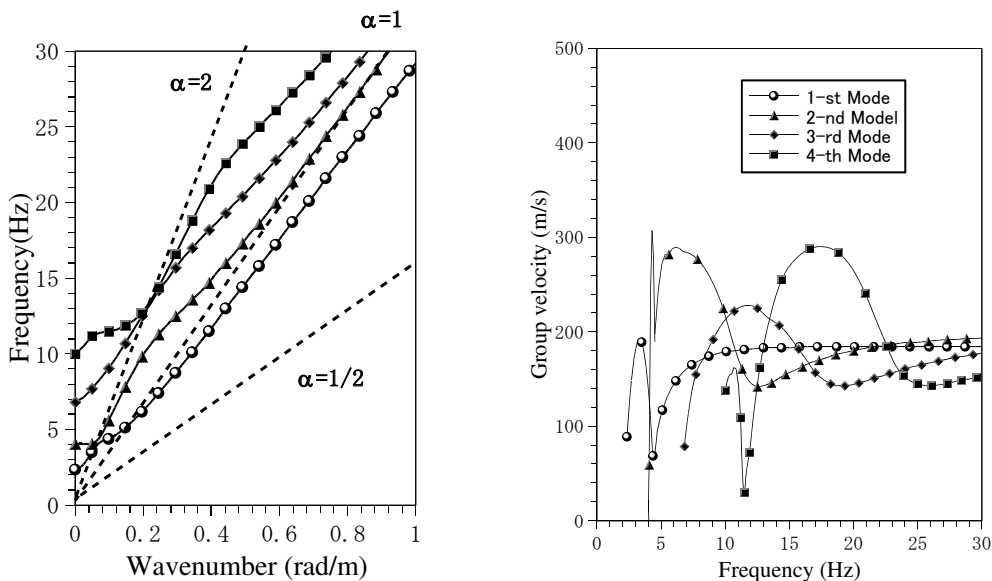


Figure 4. Wave dispersion characteristic for in-plane wave. Frequency-wave number curve (left) and group velocity-frequency curve (right).

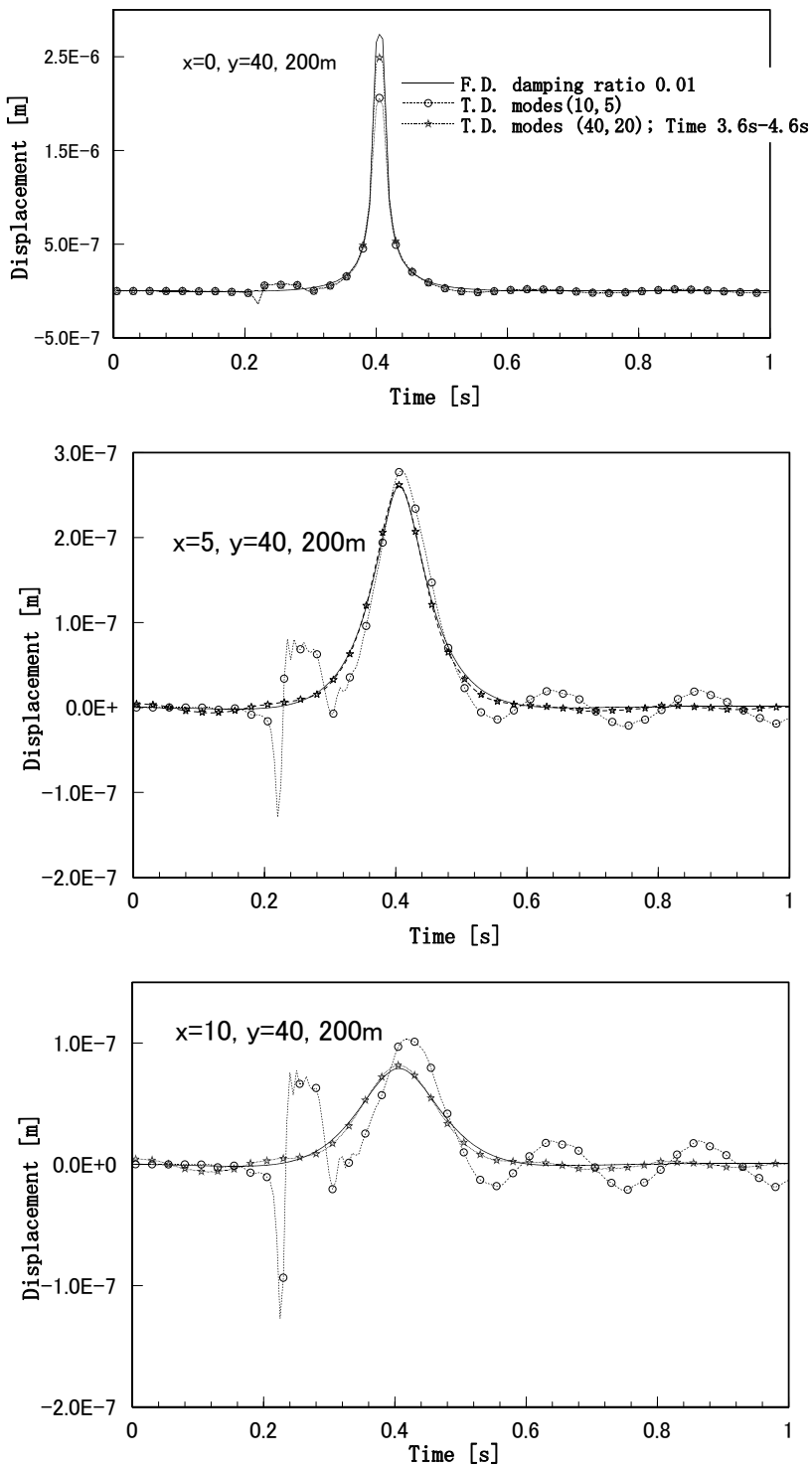


Figure 5. Transient response under a moving load for the $\alpha = 0.5$ subseismic situation.

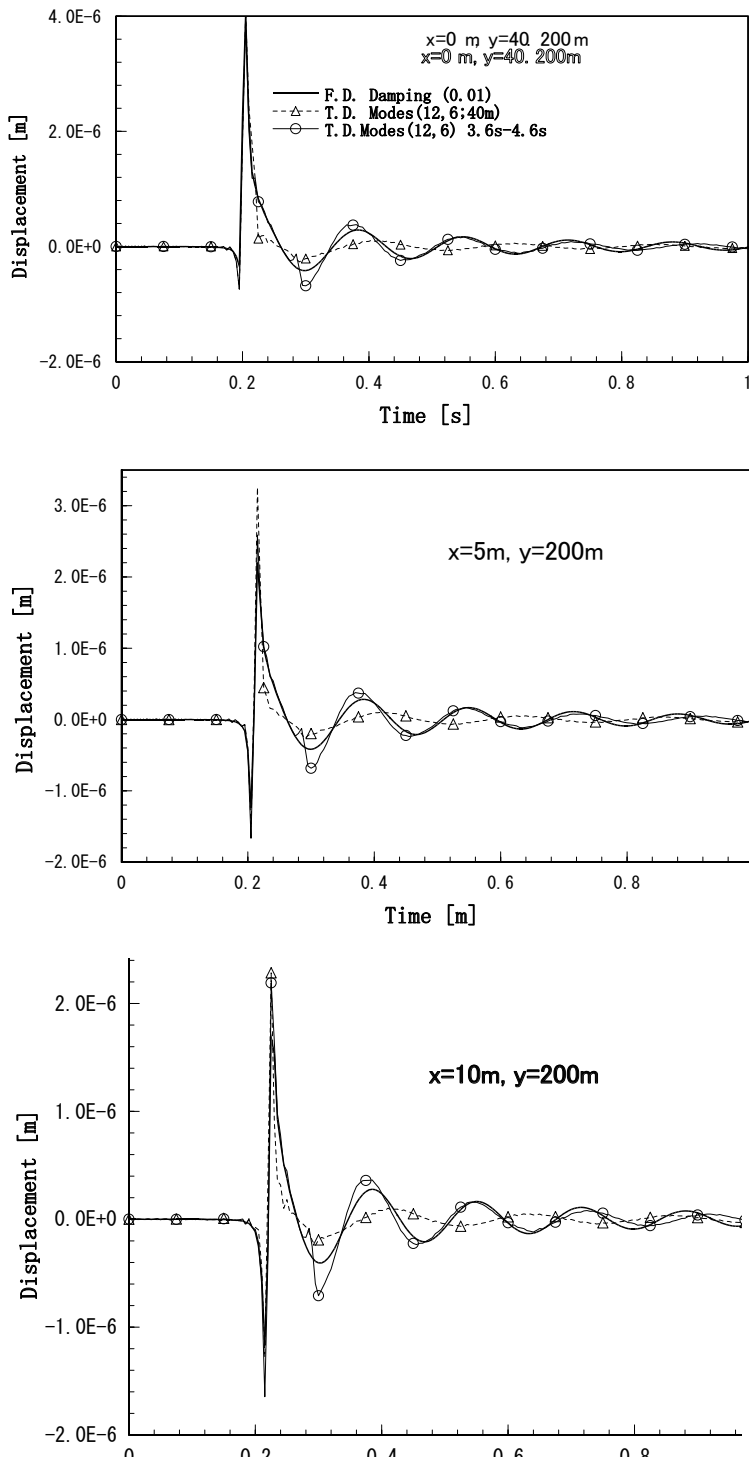


Figure 6. Transient response under a moving load for the $\alpha = 1.0$ seismic situation.

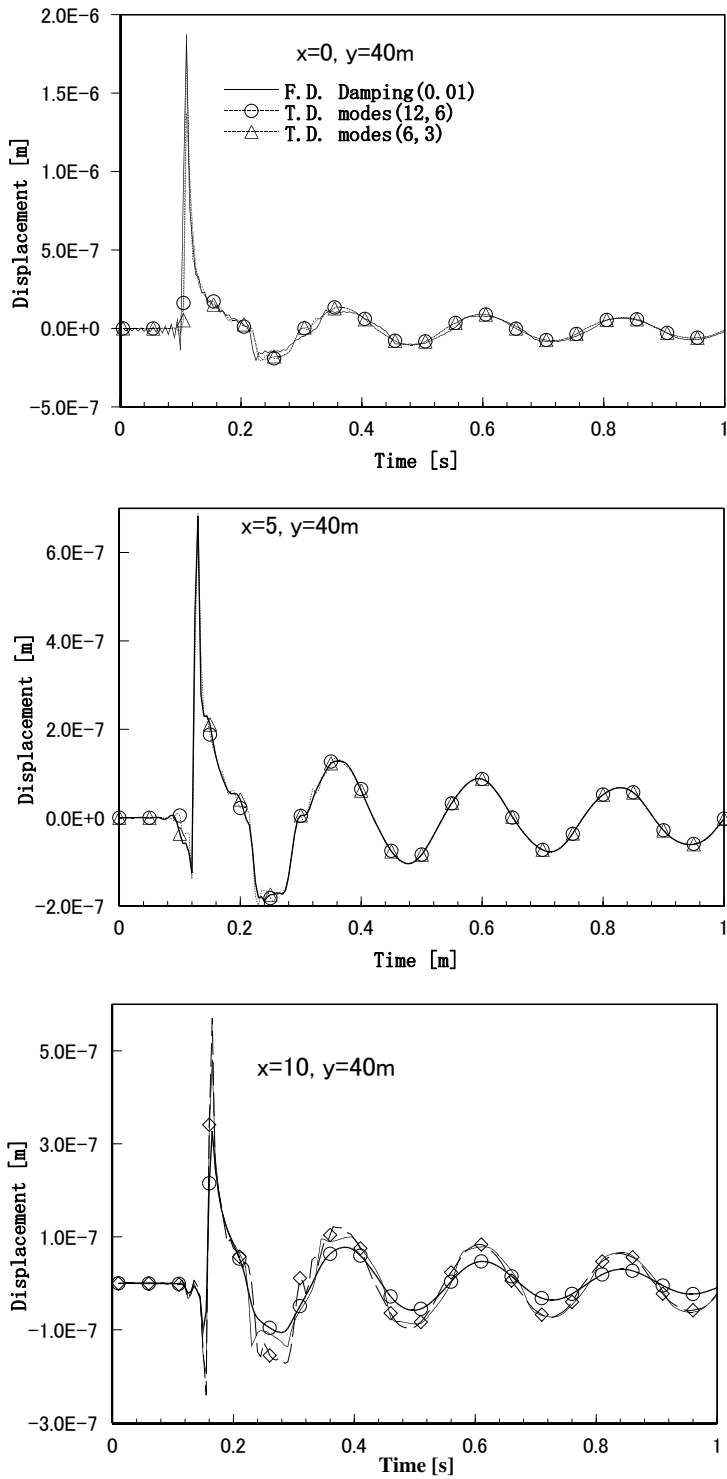


Figure 7. Transient response under a moving load for the $\alpha = 2.0$ superseismic situation.

modes used are indicated in the figure: the first number refers to the number of in-plane modes and the second number to the number of out-of-plane mode. By referring to (40), we note that the moving load has a velocity-dependent periodic nature in addition to that of the Laplace transform for the Heaviside type loading. The consequences are drastically different response features for different speeds of the moving load. For the subseismic situation with speed ratio $\alpha = 1/2$, the initial impact effect appears at an observation point ahead of the moving load at the time of seismic wave arrivals. The fronts of the P , SV , and Rayleigh waves are clearly detectable. Therefore, the former can be separated from the latter by taking a long approach, for instance 200 m, from the starting point to the observation point. The total response time histories, after the initial effect is excluded by an appropriate time window, are also depicted. They are denoted by TD with a specific time indicated. The frequency domain solutions, indicated as FD [Takemiya 2001; 2003], are also depicted in the figure for comparison. These include a nominal small damping ratio $\beta = 0.01$ for the sake of a stable computation. All the resulting FD responses, regardless of the distance off the moving line, look like kinematic ground deformations; the responses attain a maximum at the moment the load passes the observation point, with almost symmetric variation before and after it.

Next, for the seismic resonance situation of the speed ratio $\alpha = 1$, the response features are described as an impulsive response, as for a δ -type loading at the temporal position of the load, with small successive fluctuations with a specific period. This periodicity is distorted in comparison with the frequency domain solution if the observation point lies in a short distance. However, if the observation point is set as far as 200 m, then the periodicity agrees well with the 6 Hz periodicity from the frequency domain solution. This frequency was predicted from the crossing of the speed line with the first wave mode curve.

Lastly, for the superseismic situation of the speed ratio $\alpha = 2$, the direct effect of the moving load precedes the wave fronts due to the initial loading. Because of the small contribution, they are embedded in the dynamic response within the chosen time window in the figure. The respective peak values are quite similar to those in the seismic resonance case, but smaller. In contrast, the harmonic fluctuations are more conspicuous in the superseismic situation. This phenomenon may be reasoned as follows: the periodicity of the tailing response is estimated as 4 Hz, which coincides with the crossing frequency of the speed line with the first mode wave curve and furthermore corresponds to the Airy phase frequency of this wave mode.

The Fourier amplitudes of the transient responses in Figure 5–7 are depicted in Figure 8. For the speed ratio $\alpha = 0.5$, the amplitudes are almost constant in the frequency range up to several Hz. For $\alpha = 1$ or 2, it is interesting to note that a peak response due to the moving speed of the load occurs at different frequencies. For the former case it is at 5.5 Hz and for the latter case it is at 4.5 Hz. In the above low frequency range or below the peak, a significant response reduction results as the distance increases off the moving axis. This fact has been already pointed out in [Takemiya and Goda 2000] as a consequence of the cut-off frequency to be determined by the stratum depth.

5.3. Application: Track response under train passage. Another application of the TLM is applied to an actual problem to predict the response of a ballast type train track under the passage of trains. The train geometry is illustrated in Table 1 and Figure 9. The wave fields of layered soils due to the Swedish X-2000 trains of different speeds have already been analyzed in the frequency domain solution method [Takemiya 2001; Takemiya and Bian 2005]. The site condition is prescribed for the equivalent soil properties in

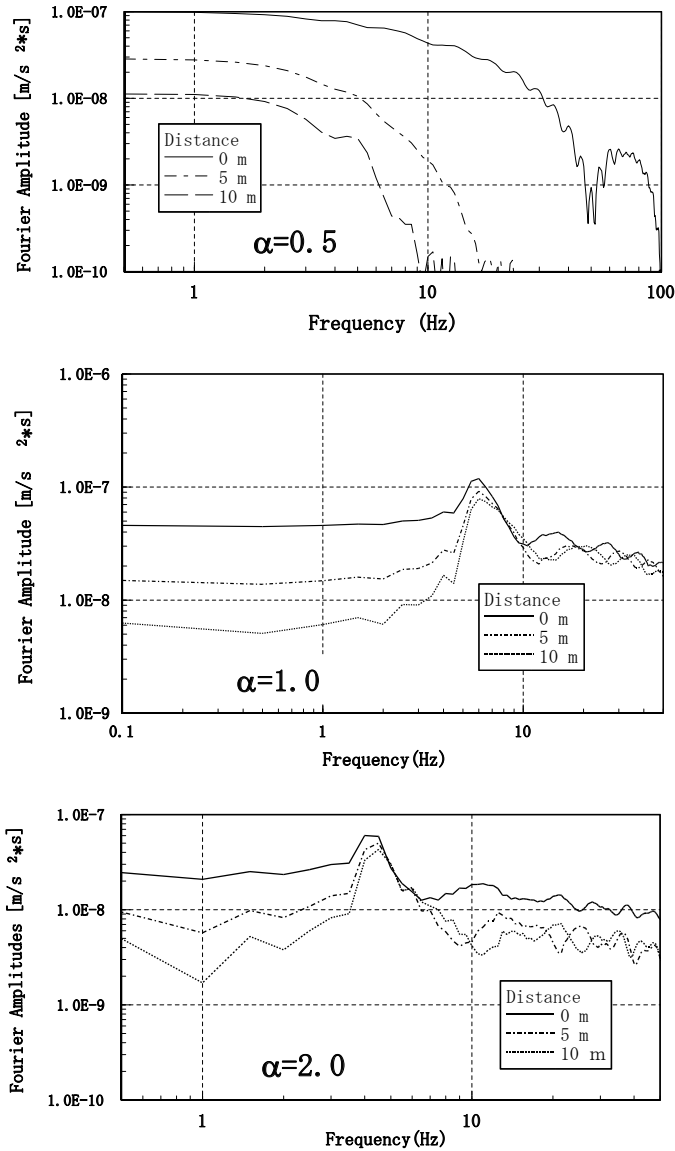


Figure 8. Fourier amplitudes of transient responses.

Train Car No (Southbound)	5	4	3	2	1
P_{n2}, P_{n1} (kN)	181.5, 180.0	122.5, 122.5	122.5, 122.5	122.5, 122.5	117.5, 160
a_n (m)	2.9	2.9	2.9	2.9	2.9
b_n (m)	6.6	14.8	14.8	14.8	11.6
L_n (m)	17.17	24.4	24.4	24.4	22.17

Table 1. Swedish X-2000 train geometry (see also Figure 9).

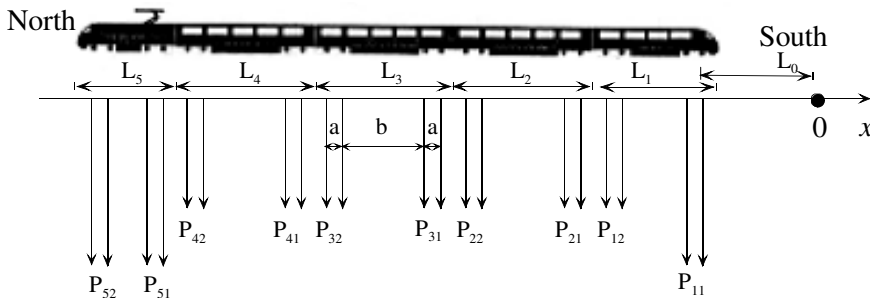


Figure 9. A train geometry, Swedish X-2000.

Table 2. Herein a stacked layered soil model is considered for the sake of the TLM computation. An additional layer of 1.4 m thickness is put at the top to approximate the track portion, and the fictitious rigid bottom base is set at 45 m depth. The employed subdivision is $4 + 10 + 9 + 12 + 45 = 80$ layers in total. An equal sublayer thickness is employed within the respective original geological layers.

The axle loading due to train passage onto the ground beneath is presumed in the form of (34) with $q = (3\pi/4)L_c = 6.2\text{ m}$ [Takemiya 2001], which means that 9 sleepers of 2 m long are involved together for a track deflection under the given rigidities of rails and ballast. This set of adjusted loads gives rise to a train load when the phase distances associated with the train geometry are properly taken into account. Since these are taken as in a stationary moving state, the causal response due to the initial condition should be excluded. For this requirement, first, the starting position of the axle load is set at 80 m in front of the focused position for the moving speed of 70 km/h, and 400 m for the moving speed of 200 km/h. The response time windows are then picked up to exclude the transient response due to the initial condition by inspection of the duration of these response time histories. Figure 10 shows the results after superposition of individual responses by following (41) for the given axle loads in Table 1. The kinematic response at low train speed is reproduced in the computation and shows a good fitting with the measurement data, although smaller peak values are predicted at the passage of the first and final axles. A dynamic response at high speed is attained which approximates the measured data quite acceptably, except for the final response to the passage of the last bogie and thereafter. This discrepancy may be caused by the track modeling in view of [Takemiya and Bian 2005] and the associated nonlinear behavior. The mechanism of the wave generation and propagation in the ground is interpreted from the wave dispersion characteristics that show the frequency versus wave number [Takemiya 2001]. In the

No	Properties	Shear Velocity (m/s)		Density (t/m^3)	Poisson ratio	Layer thickness (m)
		19.4 m/s	55.6 m/s			
1	Crust	72.0	65.0	1.5	0.49	1.1
2	Original Clay	41.0	33.0	1.26	0.49	3.0
3	Clay	65.0	60.0	1.475	0.49	4.5
4	Clay	87.0	85.0	1.475	0.49	6.0

Table 2. Soil properties at Ledsgard.

low speed situation, the train speed line is off-set lower than the fundamental wave mode line, whereas in the latter situation it indicates the crossing of the speed line with the fundamental wave mode line at 2.5 Hz, the corresponding wavelength is 16.7 m. These facts are confirmed in Figure 10.

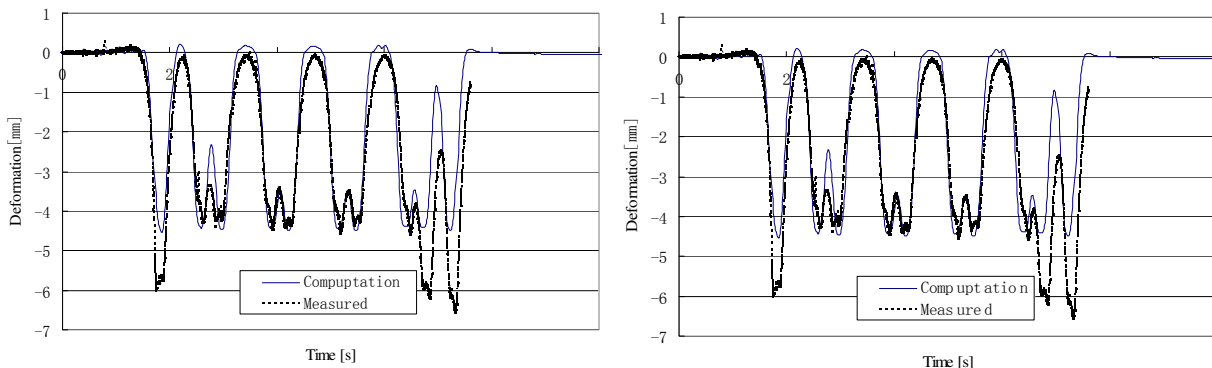


Figure 10. Track response due to the X2000 train passage at (left) 70 km/h (19.4 m/s) and (right) 200 km/h (55.6 m/s).

6. Conclusions

The transient responses due to moving loads, initially at rest, have been dealt with by the Laplace–Fourier transform scheme with respect to time and space, respectively. The TLM is applied for discretization along the depth of the ground. The wave field can be decomposed into the eigenmodes of wave numbers in the horizontal dependence once it is decoupled into in-plane and out-of-plane motions. A variety of space distributions and time variations are considered for loading profiles.

Firstly, an illustrative study is demonstrated for the transient response of a uniform halfspace due to sudden vertical loading on the surface. The causal responses of the TLM are validated in comparison with the closed form solution.

Secondly, the transient response due to a constant moving (quasistatic) load is investigated for a stratum model. The causality features are discussed depending on the speed ratio of the moving load against the shear velocity of the layer. From the computed results, it is noted that in the case of a short distance from a starting position to an observation position, the wave field includes the initial touch down effect as well as the moving load effect. However, as the distance is increased, the former response becomes substantially separated from the latter response. Regarding the speed ratio of the moving load against the seismic S wave velocity, distinct response features result. Those are interpreted in the time as well as in the frequency domains. The wave dispersion characteristics are helpful to give a fundamental knowledge for predicting the ground borne vibration.

Thirdly, a practical application is attempted to predict train-induced vibration. Since the stationary response is focused on a constant speed passage, the superposition is taken for a set of responses due to axle loads, with special care to exclude the causal effects from the initial condition. The validation is made from the measured data at the site.

Notation

A, B, C	coefficient matrices
$c_{\text{P-SV}}$	train speed
$\tilde{\mathbf{E}}^{\text{P-SV}}, \tilde{\mathbf{E}}^{\text{SH}}$	diagonal matrices defined in (19) and (20)
$\tilde{\mathbf{F}}_1, \tilde{\mathbf{F}}_2, \tilde{\mathbf{F}}_3$	force vectors in the Fourier transformed domain
$H(t)$	Heaviside step function
L	fundamental wavelength
M	mass matrix
s	Laplace parameter
s_j	wave number eigenvalue
$T(t)$	time function
$\tilde{T}(s)$	Laplace transform of time function
\mathbf{U}	nodal displacement vector
$\tilde{\mathbf{U}}_1, \tilde{\mathbf{U}}_2, \tilde{\mathbf{U}}_3$	Fourier–Laplace transformed displacements
β	damping ratio
$\Lambda^{\text{P-SV}}, \Lambda^{\text{SH}}$	diagonal matrices eigenwave numbers for waves field as P-SV and SH
ξ	wave number
Φ	mode shape matrix
$\delta(\)$	Dirac delta function
ρ	density
ω	circular frequency
$-$	Laplace transform with respect to time
\sim	Fourier transform with respect to space coordinate

Acknowledgement

The author expresses his thanks to S. Yagi for implementing the theory involved into a computer code, and also to Dr. F. Chen for some recomputation of examples shown here.

References

- [Dieterman and Metrikine 1997] H. A. Dieterman and A. V. Metrikine, “Steady-state displacements of a beam on an elastic half-space due to a uniformly moving constant load”, *Eur. J. Mech. A Solids* **6**:2 (1997), 295–306.
- [Eason 1965] G. Eason, “The stresses produced in a semi-infinite solid by a moving surface force”, *Int. J. Eng. Sci.* **2**:6 (1965), 581–609.
- [Eason 1966] G. Eason, “The displacements produced in an elastic half-space by a suddenly applied surface force”, *J. Inst. Math. Appl.* **2** (1966), 299–326. MR 34 #5361
- [Gakenheimer and Miklowitz 1969] D. C. Gakenheimer and J. Miklowitz, “Transient excitation of an elastic halfspace by a point load traveling on the surface”, *J. Appl. Mech. (ASME)* **36**:3 (1969), 505–515.
- [Haddon 1987] R. A. W. Haddon, “A simple exact method for Green’s functions for SH motion in a layered elastic medium using leaking modes”, *Geophys. J. Int.* **88**:2 (1987), 379–392.
- [Harvey 1981] D. J. Harvey, “Seismogram synthesis using normal mode superposition: The locked mode approximation”, *Geophys. J. Int.* **66**:1 (1981), 37–69.
- [Kausel 1994] E. Kausel, “Thin-layer method: Formulation in the time domain”, *Int. J. Numer. Methods Eng.* **37**:6 (1994), 927–941.

- [Kausel et al. 1975] E. Kausel, J. M. Roesset, and G. Waas, “Dynamic analysis of footings on layered media”, *J. Eng. Mech. (ASCE)* **101**:5 (1975), 679–693.
- [Lamb 1904] H. Lamb, “On the propagation of tremors over the surface of an elastic solid”, *Philos. Tr. R. Soc. S. A* **203** (1904), 1–42.
- [Lombaert et al. 2001] G. Lombaert, G. Degrande, and D. Clouteau, “The influence of the soil stratification on free field traffic-induced vibrations”, *Arch. Appl. Mech.* **71**:10 (2001), 661–678.
- [Lysmer and Drake 1972] J. Lysmer and L. A. Drake, “A finite element method for seismology”, *Methods Comput. Phys.* **11** (1972), 181–216.
- [Mitra 1964] M. Mitra, “Disturbance produced in an elastic half-space by impulsive normal pressure”, *Proc. Camb. Philos. Soc.* **60** (1964), 683–696. MR 29 #5458
- [Olson et al. 1984] A. H. Olson, J. A. Orcutt, and G. A. Frazier, “The discrete wavenumber/finite element method for synthetic seismograms”, *Geophys. J. Int.* **77**:2 (1984), 421–460.
- [Payton 1964] R. G. Payton, “An application of the dynamic Betti–Rayleigh reciprocal theorem to moving-point loads in elastic media”, *Quart. Appl. Math.* **21**:4 (1964), 299–313. MR 27 #5411
- [Pekeris 1955] C. L. Pekeris, “The seismic buried pulse”, *Proc. Nat. Acad. Sci. U.S.A.* **41**:9 (1955), 629–639. MR 17,320e
- [Sheng et al. 1999] X. Sheng, C. J. C. Jones, and M. Petyt, “Ground vibration generated by a harmonic load acting on a railway track”, *J. Sound Vib.* **225**:1 (1999), 3–28.
- [Takemiya 2001] H. Takemiya, “Noise and vibration from high-speed trains”, Chapter 12, pp. 347–393 in *Ground vibrations alongside tracks induced by high-speed trains: Prediction and mitigation*, edited by V. V. Krylov, Thomas Telford, London, 2001.
- [Takemiya 2003] H. Takemiya, “Simulation of track-ground vibrations due to a high-speed train: The case of X-2000 at Ledsgard”, *J. Sound Vib.* **261**:3 (2003), 503–526.
- [Takemiya and Bian 2005] H. Takemiya and X. C. Bian, “Substructure simulation of inhomogeneous track and layered ground dynamic interaction under train passage”, *J. Eng. Mech. (ASCE)* **131**:7 (2005), 699–711.
- [Takemiya and Fujiwara 1994] H. Takemiya and A. Fujiwara, “Wave propagation/impediment in a stratum and wave impeding block (WIB) measured for SSI response reduction”, *Soil Dyn. Earthq. Eng.* **13**:1 (1994), 49–61.
- [Takemiya and Goda 2000] H. Takemiya and K. Goda, “Thin layer method simulation of near source ground motions due to discretized dislocation in layered soils”, *J. Struct. Mech. Earthq. Eng. (JSCE)* **640**:50 (2000), 89–98.
- [Takemiya and Guan 1993] H. Takemiya and F. Guan, “Transient Lamb’s solution for surface strip impulses”, *J. Eng. Mech. (ASCE)* **119**:12 (1993), 2385–2403.
- [Takemiya and Steinfeld 1993] H. Takemiya and B. Steinfeld, “Transient 3D Lamb’s solution by classical approach and direct boundary element method”, pp. 307–314 in *Proceedings of the Second European Conference on Structural Dynamics (EURODYN ’93)* (Trondheim), edited by T. Moan et al., Balkema, Rotterdam, 1993.
- [Takemiya et al. 1994] H. Takemiya, F. Guan, and Y. Sukeyasu, “2-D transient soil-surface foundation interaction and wave propagation by time domain BEM”, *Earthquake Eng. Struct. Dyn.* **23**:9 (1994), 931–945.
- [Takemiya et al. 2001] H. Takemiya, S. Satonaka, and W. P. Xie, “Train-track-ground dynamics due to high speed moving source and ground vibration transmission”, *J. Struct. Mech. Earthq. Eng. (JSCE)* **882**:56 (2001), 299–309.
- [Touhei 1995] T. Touhei, “Propagation of normal modes due to impulsive loading to 3-D medium on a rigid basement”, *Earthquake Eng. Struct. Dyn.* **24**:7 (1995), 937–949.

Received 1 Jun 2007. Revised 23 Nov 2007. Accepted 6 Dec 2007.

HIROKAZU TAKEMIYA: takemiya@ed-techno.org
E&D Techno-design, Inc., Haga 5303, Okayama, Japan